Ab Initio Study of NMR ^{15}N Chemical Shift Differences Induced by Ca^{2+} Binding to EF-Hand Proteins†

Rodolfo R. Biekofsky,*,‡ Adrián G. Turjanski,§ Darío A. Estrin,§ James Feeney,‡ and Annalisa Pastore‡

Molecular Structure Division, National Institute for Medical Research, The Ridgeway, Mill Hill, London NW7 1AA, United Kingdom, and Departamento de Química Inorgánica, Analítica y Química-Física e INQUIMAE, Facultad de Ciencias Exactas y Naturales, Universidad de Buenos Aires, Ciudad Universitaria, Pab. 2, C1428EHA, Buenos Aires, Argentina

Received January 30, 2004; Revised Manuscript Received March 9, 2004

ABSTRACT: EF-hands are Ca^{2+} binding motifs that are widely distributed throughout the entire living organism kingdom. At present, relatively little is known at a quantum mechanical level about the mechanisms that allow Ca^{2+} to be recognized specifically by EF-hands and to induce a conformational switch from a compact ("closed") conformation to an "open" state that exposes a large patch of hydrophobic residues. Here, we present a study of NMR ^{15}N chemical shifts based on ab initio quantum mechanical calculations carried out on a minimalist model system linking both Ca^{2+} binding sites across the β-sheet of an EF-hand domain. Calculated and experimentally determined chemical shift changes are correlated with structural changes induced upon metal binding. The effect of Ca^{2+} binding on these ^{15}N shifts can be dissected into two main contributions: one from π-polarization of β-sheet amide groups and the other from rotation of an isoleucine side chain. By correlating this description with experimental evidence, different polarization states for the β-sheet amide groups were identified and linked to the overall conformation of different EF-hand domains. When all four β-sheet amide groups are polarized, the ab initio calculations in our model indicate a cooperative stabilization effect due to the establishment of a circular network of donor-acceptor interactions connecting the two Ca^{2+} ions across the β-sheet. The emerging hypothesis from our analysis is that this cooperative network of interactions is essential for stabilizing the "open" conformation of an EF-hand domain.

Calcium ions, essential for many biological functions, are known to act as second signaling messengers in the cell (*1*). One of the most common calcium binding scaffolds in proteins is the EF-hand, which consists of a helix-loop-helix motif made up of 29 consecutive residues, with two α-helices flanking a 12-residue Ca^{2+} binding loop (Figure 1A) (*2*). EF-hands normally occur in pairs that form four helix bundle globular domains.

The binding of Ca^{2+} involves a structural rearrangement of the four α-helices of the EF-hand pair domain with the consequent exposure of a hydrophobic cleft (Figure 1B), often referred to as the "Ca^{2+} switch" (*3*−*10*). The exposed hydrophobic pocket can then interact with other proteins in the cell, thereby modulating their function (*11*). In this way, a Ca^{2+} binary signal (Ca^{2+} on/Ca^{2+} off) is initiated, thus enabling the cell to control biological processes as diverse as muscle contraction, fertilization, cell proliferation, vesicular fusion, and apoptosis (*1*). CaM,[1] probably the best paradigm of EF-hand proteins, consists of two such globular domains linked by a flexible tether, each domain capable of binding selectively two Ca^{2+} ions with positive cooperativity (*12*).

Despite the biological importance of the Ca^{2+} switch, many questions still remain unanswered about this mechanism: What are the determinants that allow EF-hand proteins to bind Ca^{2+} selectively even in the presence of high concentrations of Mg^{2+}? What are the forces that trigger the closed-to-open conformational switch? Is the cooperativity of Ca^{2+} binding related to this dramatic conformational change? A vast plethora of experimental work has been published addressing these questions and identifying residues that appear to play a role in EF-hand/metal recognition. However, there is still no theoretical description of the system that would allow us to fully understand the atomic details of this mechanism and its biological consequences.

The so-called EF-hand loop is a 12 residue segment that contains all of the calcium binding ligands (see Figure 2A) (*13*). The calcium ion is coordinated by seven oxygens: monodentate carboxylate or carboxamide ligands are in positions 1, 3, and 5 of the loop; a backbone carbonyl ligand is in position 7; and a universally conserved glutamate is in position 12. The γ-carboxylate of this glutamate coordinates to the Ca^{2+} ion in a bidentate manner, i.e., using both carboxylate oxygen atoms. A water molecule generally provides the seventh oxygen ligand for the Ca^{2+} ion.

† D.A.E. and A.G.T. acknowledge Fundacion Antorchas, Universidad de Buenos Aires, and ANPCYT for financial support. They are also indebted to Pablo de Grande, Microsoft Argentina, and the LBP Endowment for Sciences and Arts for generous donations.

* To whom correspondence should be addressed. Tel: 44-20-8959-3666. Fax: 44-20-8906-4477. E-mail: rbiekof@nimr.mrc.ac.uk.

‡ National Institute for Medical Research.

§ Universidad de Buenos Aires.

[1] Abbreviations: BSSE, basis set superposition errors; CaM, calmodulin; cTnC, cardiac troponin C; DFT, density functional perturbation theory; NMR, nuclear magnetic resonance; NOE, nuclear Overhauser effect; sTnC, skeletal troponin C; TnC, troponin C.

10.1021/bi0497852 CCC: $27.50
Published on Web 05/06/2004

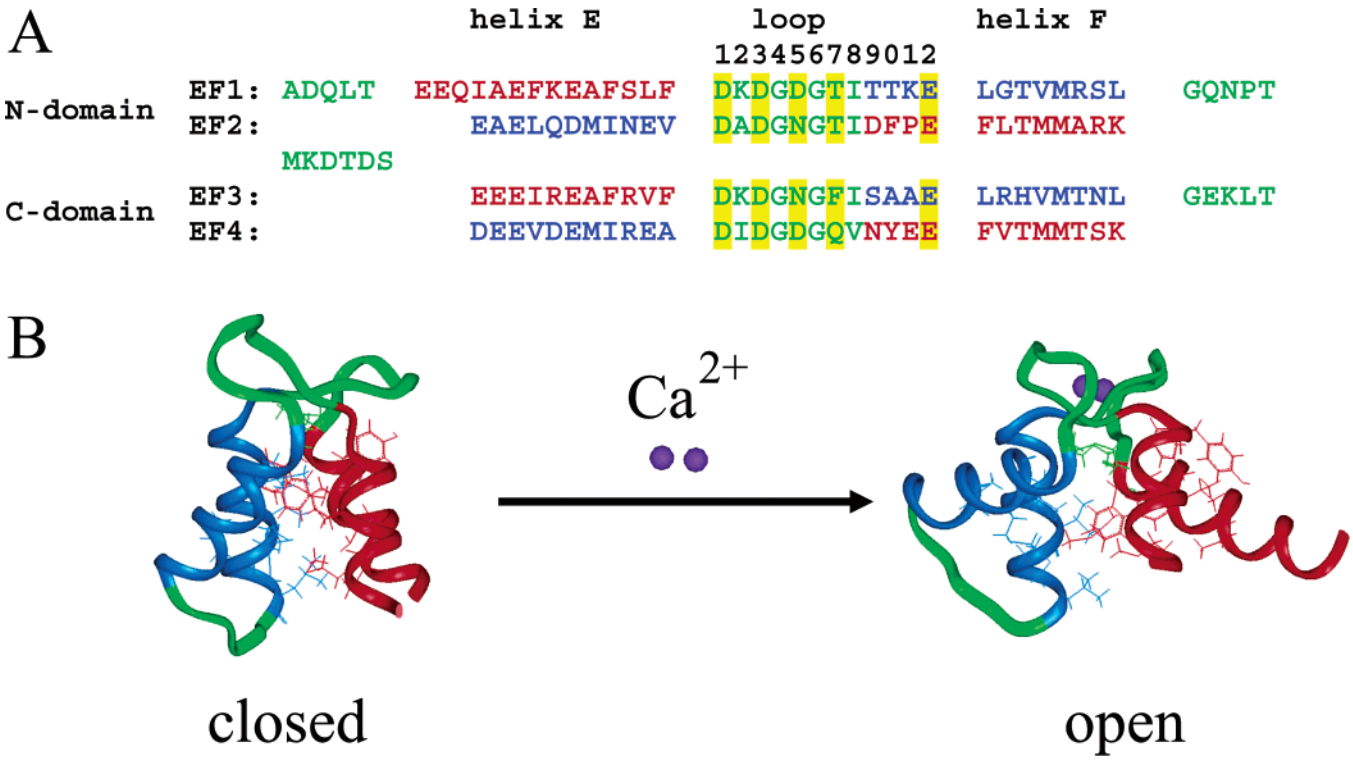

FIGURE 1: (A) Sequence alignment of the four EF-hands of CaM, indicated as EF1−4. The helix-loop-helix motifs are indicated on the top of the sequences, as well as the canonical positions of the EF-hand loop. Ca^{2+} is chelated through seven oxygen atoms arranged three-dimensionally on the axes of a pentagonal bipyramid (*78*): the oxygens of the carbonyl groups for residues in positions 1, 3, 5, and 7, both oxygens of the side chain carboxylate group in position 12 of the loop, and an oxygen from a water molecule. The protein residues providing ligands are indicated with yellow boxes. (B) Conformational switch of a representative EF-hand domain upon Ca^{2+} binding. In the absence of Ca^{2+} (closed state), the four helices form a compact four helix bundle. The two loops are linked back to back by a short antiparallel β-sheet. Upon Ca^{2+} binding to the loops, the structure opens up (open state), keeping helix A (EF1) paired to helix D (EF2) (shown in red) and helix B (EF1) paired to helix C (EF2) (shown in blue). This movement exposes the hydrophobic core of the domain, which can then interact with a protein partner. Shown here are the structures of the C-terminal domain of CaM in its apo (PDB accession code: 1F71) (*35*) and holo forms (PDB accession code: 1EXR) (*63*). The side chains of hydrophobic residues are shown in both apo and holo forms.

A few years ago, in a systematic examination of NMR chemical shifts from a number of EF-hand proteins, we showed that certain ^{15}N shifts change greatly upon Ca^{2+} binding (*14*). In particular, upon Ca^{2+} coordination to the backbone carbonyl in position 7, there is an appreciable deshielding of the amide ^{15}N nucleus at position 8 (+4 to +8 ppm). This deshielding effect is effectively independent of the binding of Ca^{2+} to the paired site of an EF-hand domain, allowing the ^{15}N shifts to be used as probes for site specific occupancy of metal binding sites. These ^{15}N chemical shift differences have proved useful for characterizing metal binding to new Ca^{2+} binding proteins (*15*−*24*) and for investigating Ca^{2+} binding in different EF-hand systems (*25*−*29*). However, the straightforward interpretation of these ^{15}N shifts is complicated by the existence of another important effect related to the binding of Ca^{2+} that is not site specific (*14*). An appreciable deshielding of the ^{15}N nucleus at position 8 (a +6 to +8 ppm) was also observed upon a change in the side chain χ_1 torsion angle of the residue in position 8, normally a conserved isoluecine or valine residue. This deshielding effect has only been observed for position 8 residues of the first EF-hand (EF1), changing from a *gauche(−)* conformation in the Ca^{2+}-free (apo) state to a *trans* conformation in the Ca^{2+}-bound (holo) state (*14*) (as shown in Figure 3). Given the predictive power of the position 8 ^{15}N chemical shifts, it is of practical importance to provide a theoretical framework for the better understanding of the determinants underlying the chemical shift changes. Our preliminary theoretical study indicated that electronic changes in residues 8 and 9 upon Ca^{2+} binding to both sites of an EF-hand domain are related to the cooperativity of Ca^{2+} binding (*30*).

The present work investigates the origins of the Ca^{2+}-induced ^{15}N chemical shift changes for positions 8 and 9 by using an ab initio approach in the framework of DFT on a model system. Progress in the field of quantum chemistry has made possible nuclear shielding calculations of useful accuracy and reliability on fragments of biomolecules of considerable size (*31*−*34*). In this way, the calculated shieldings, as well as the calculated electronic and geometric changes introduced by the metal/ligand interactions, can be directly correlated and compared to experimental data thus providing a powerful way of translating observed chemical shift behavior into structural descriptors. These calculations provide the theoretical basis for the use of these diagnostic ^{15}N chemical shifts as an aid in assessing the site specific occupation of Ca^{2+} binding sites, rendering a better understanding of the underlying interactions determining the conformational changes associated with the binding of Ca^{2+} in this family of proteins.

RESULTS

Choice of the Model System. To rationalize the observed ^{15}N chemical shift changes upon Ca^{2+} binding from a theoretical viewpoint, we have chosen to calculate the ^{15}N

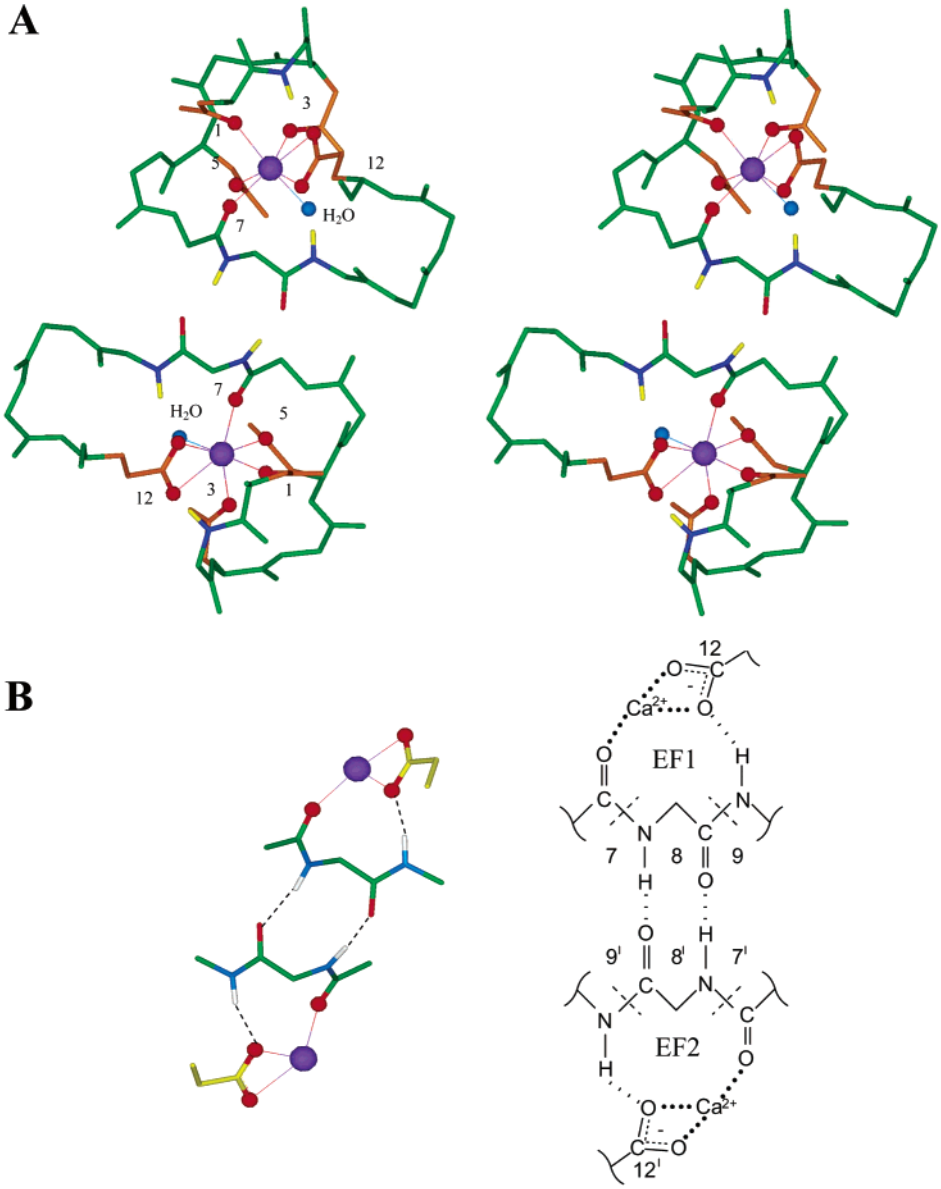

FIGURE 2: (A) Stereo representation of the three-dimensional structure of the Ca^{2+} coordination [C-terminal domain of CaM from 1EXR (*63*)]: for each EF-hand, Ca^{2+} coordination involves the six ligands in loop positions 1, 3, 5, 7, and 12 (cf. Figure 1A). A water molecule is the seventh ligand. Ca^{2+} ligating oxygen atoms are indicated using ball representations: in red are those corresponding to protein ligands, and in light blue is that corresponding to the water molecule. Ca^{2+} ions are indicated in ball representation in a violet color. NH groups involved in the cyclic network are shown in dark blue (nitrogen atoms) and yellow (hydrogen atoms), and carboxyl oxygen atoms involved in the cycle are shown in red. A hydrogen bond between the backbone amide of the residue in position 2 and one of the bidentate glutamate oxygens is also shown. (B) Three-dimensional (left) and two-dimensional schematic (right) representation of the cyclic network of interactions used in the present paper. Hydrogen bonds are indicated by slashed lines.

shieldings on Ca^{2+}-loaded (holo) and Ca^{2+}-free (apo) model systems. As shown in Figure 2A, the two calcium binding sites in EF-hand pair domains (EF1 and EF2) are structurally linked via a short antiparallel β-sheet (*7*−*10*, *13*, *35*) formed mainly between two typically conserved isoleucine residues in position 8, one from each strand of the EF-hand loops. We will refer to the residues in EF1 with unprimed numbers and to those in EF2 with primed ones. The model that we chose comprises basically the four β-sheet amide groups (from residues in positions 7−8−9 and their symmetrical residues 7′−8′−9′), plus a bidentate carboxylate (from residues in position 12 and 12′) for the holo model as shown in Figure 2B.

Two main conformations were considered for the isoleucine residue in position 8: a *gauche(−)* ($H_\alpha-C_\alpha-C_\beta-H_\beta$ torsion angle of −60°) and a *trans* conformation ($H_\alpha-C_\alpha-C_\beta-H_\beta$ torsion angle of −180°). The isoleucine residue in position 8′ was considered only in a *trans* conformation ($H_\alpha-C_\alpha-C_\beta-H_\beta$ torsion angle of −180°) since there is no experimental evidence of conformational changes for this residue upon Ca^{2+} binding (*14*). The geometries of the models were optimized before using them to investigate the ^{15}N shielding effects.

Amide Group Polarization Effect. (i) Calculation of ^{15}N Nuclear Shieldings. The effect of Ca^{2+} binding on each nitrogen atom for the model system was calculated as the difference of the ^{15}N nuclear shieldings for the apo and holo models. To separate this effect from side chain rotation effects, no changes of the χ_1 torsion angle were included in these calculations (*trans*−*trans* conformations were consid-

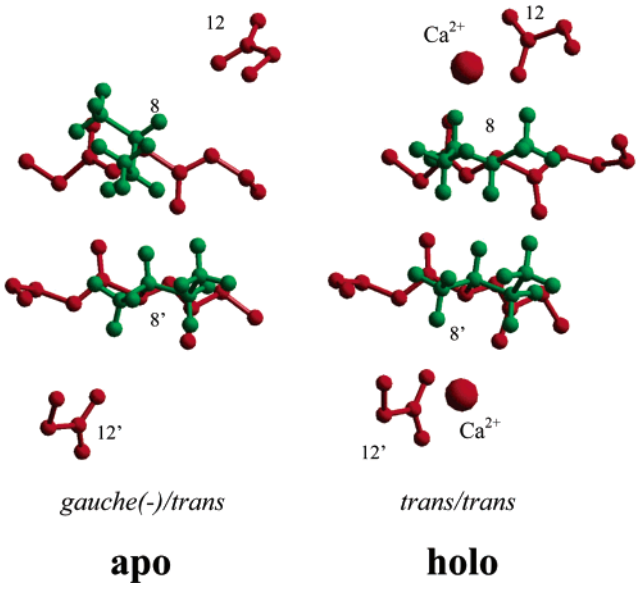

FIGURE 3: Side chain χ_1 angle of the conserved isoleucine in position 8 (EF1) is usually in a *gauche(−)* conformation in Ca^{2+}-free EF-hands. Steric hindrance forces rotation of this angle to that of a *trans* conformation upon Ca^{2+} binding on EF2. As a consequence, the chemical shift variation observed upon Ca^{2+} binding is the effect of two components, one due to bond polarization and the other to the *gauche(−)* to *trans* transition. The χ_1 angle of the conserved isoleucine in position 8′ has been observed to be in a *trans* conformation in both Ca^{2+}-free and Ca^{2+}-bound EF-hands. The figure shows the isoleucine 8 and 8′ conformation of the N-terminal domain of CaM in the apo [left; PDB access 1F70 (*35*)] and holo [right; PDB access 1EXR (*63*)] states. The isoleucine side chains are shown in green, and the rest of the molecule is in red.

ered for isoleucines in positions 8 and 8′ for apo and holo systems) (Table 1A). An appreciable deshielding of the amide nitrogens in positions 8, 9, 8′, and 9′ is observed in the holo system with respect to their values in the apo form. The values obtained for the equivalent positions 8 and 8′ and for 9 and 9′ are approximately the same as expected from the quasi *C*2 symmetry of the system. The effects obtained for N(8) and N(8′) are larger than those for N(9) and N(9′) (15.3 and 7.3 ppm, respectively) probably because O(7)═C(7)−N(8) and O(7′)═C(7′)−N(8′) amide groups interact directly with the Ca^{2+} ion through coordination of the backbone carbonyls O(7)═C(7) and O(7′)═C(7′).

The chemical shielding tensor is a symmetric second-rank tensor and can thus be described by three principal components: $\sigma 11$, $\sigma 22$, and $\sigma 33$. The differences observed in the shielding tensors are due to changes in the value of all of its components. We have evaluated the changes in these components and calculated the spans ($\Omega = \sigma 33 - \sigma 11$), as a measure of the anisotropy of the tensor. For N(8) and N(8′), the change is uniform, while for N(9) and N(9′) there is an increase in $\sigma 11$ and $\sigma 22$ and no trend in $\sigma 33$ upon Ca^{2+} binding. The spans are bigger for N(8) and N(8′) than for N(9) and N(9′); however, the change in the ^{15}N spans when going from apo to holo is greater for N(9), N(9′) than for N(8), N(8′).

(ii) Comparison with the ^{15}N Experimental Values. The calculated ^{15}N shieldings shown in Table 1A for positions 8, 8′, and 9, 9′ (average +15.3 and +7.3 ppm, respectively) are in agreement with the trends observed in the experimental values; however, they are somewhat larger than the observed

Table 1: Calculated ^{15}N Shieldings[a] for β-Sheet Amide Groups

A: Effect of Ca^{2+} Binding on the Nitrogens in Positions 8, 9 (EF1) and 8′, 9′ (EF2)

		N(8)	N(9)	N(8′)	N(9′)
holo	*trans−trans*	103.9	84.5	104.8	83.9
apo	*trans−trans*	88.8	76.8	89.2	76.8
calculated $\Delta\delta_{polariz}$[b]		+15.1	+7.7	+15.6	+7.1

B: Effect of the $\chi 1$ Rotation of Ile(8) of EF1 from *gauche(−)* to *trans*

		N(8)	N(9)	N(8′)	N(9′)
apo	*trans−trans*	88.8	76.8	89.2	76.8
apo	*gauche(−)−trans*	81.8	72.6	88.1	76.6
calculated $\Delta\delta_{rotation}$[c]		+7.0	+4.2	+1.1	+0.2

C: Combined Effect of Ca^{2+} Binding to EF1 and EF2 and $\chi 1$ Rotation of Ile(8) of EF1 from *gauche(−)* to *trans*

		N(8)	N(9)	N(8′)	N(9′)
holo	*trans−trans*	103.9	84.5	104.8	83.9
apo	*gauche(−)−trans*	81.8	72.6	88.1	76.6
calculated $\Delta\delta_{total}$[d]		+22.1	+11.9	+16.7	+7.3

[a] In parts per million (ppm). [b] $\Delta\delta_{polariz} = \delta_{holo} - \delta_{apo}$; polarization contribution to the ^{15}N chemical shielding calculated as the difference between ^{15}N chemical shieldings for the *trans/trans* holo and *trans/trans* apo models. [c] $\Delta\delta_{rotation} = \delta_{trans/trans} - \delta_{gauche/trans}$; rotation contribution to the ^{15}N chemical shielding calculated as the difference between ^{15}N chemical shieldings for the *trans/trans* and *gauche(−)/trans* apo models. [d] $\Delta\delta_{total} = \delta_{holo} - \delta_{apo}$; difference between ^{15}N chemical shieldings for the *trans/trans* holo and *gauche(−)/trans* apo models. $\Delta\delta_{total} = \Delta\delta_{polariz} + \Delta\delta_{rotation}$; $\Delta\delta_{total}$ is the sum of both contributions.

experimental values (+6.1 and +4.3 ppm, as shown in Table 2A for 8′ and 9′, respectively). We suspect that the approximation of neglecting the rest of the molecule (particularly the other Ca^{2+} ligands) results in an overestimation of the calculated polarization contribution.

(iii) Origin of the ^{15}N Deshielding Effects. Our ab initio calculations show that the ^{15}N deshielding caused by Ca^{2+} binding mainly originates from polarization of the amide groups. There is also a charge transfer from the protein to the Ca^{2+} atoms that increases the polarization effect. The predicted concurrent lengthening of the O−C and N−H bonds and the shortening of the C═N bonds of the four β-sheet amide groups upon Ca^{2+} binding (Table 3A) imply an increase of partial double-bond character of the amide bond. The increase of π-electron density of the oxygen atoms and the decrease of π-electron density of the nitrogen atoms (Table 3B and Figure 4) are consistent with simultaneous polarization of the four β-sheet amide groups upon Ca^{2+} binding. In the case of O(7)═C(7)−N(8) and O(7′)═C(7′)−N(8′) amide groups, the polarization occurs upon coordination of the backbone carbonyl to the Ca^{2+} ion. In the case of the O(8)═C(8)−N(9) amide group [and similarly for the O(8′)═C(8′)−N(9′) amide group], the polarization occurs upon formation of a hydrogen bond between N(9) and H(9) with an oxygen of the carboxylate of glutamate(12), which coordinates to the Ca^{2+} ion in a bidentate manner.

The hydrogen bond interactions between the two β-sheet strands are predicted to become tighter upon Ca^{2+} binding, as seen from the calculated shortening of the H(8)···O(8′) and H(8′)···O(8) distances (Table 3A) and from the increased polarization of the hydrogen and oxygen atom [the electronic density on the O(8) and O(8′) atoms increases and that on the H(8) and H(8′) decreases] (Figure 4A,B). This result is

Table 2: Experimental ^{15}N Chemical Shift Differences (in ppm) for the NH Groups in Positions 8, 9, 8′, 9′ of the EF-Hand Loops between Holo and Apo Forms of Different Calcium Binding Proteins

		EF1		EF2	
EF-domain		N(8)[a]	N(9)[a]	N(8′)[a]	N(9′)[a]
A: binding of Ca^{2+} to both EF-hands					
N-CaM[f,g]		Ile27	Thr28	Ile63	Asp64
	$\delta(Ca_2)$[b]	127.1	116.6	124.0	128.3
	δ(apo)[c]	111.0	111.2	119.8	124.6
	$\Delta\delta(Ca_2\text{-apo})$[d]	+16.1	+5.4	+4.2	+3.7
C-CaM[f,g]		Ile100	Ser101	Val136	Asn137
	$\delta(Ca_2)$[b]	127.3	123.8	125.2	129.0
	δ(apo)[c]	113.9	118.0	120.0	125.7
	$\Delta\delta(Ca_2\text{-apo})$[d]	+13.4	+5.8	+5.2	+3.3
N-TnC[h]		Ile37	Ser38	Ile73	Asp74
	$\delta(Ca_2)$[b]	125.9	124.0	126.5	131.9
	δ(apo)[c]	111.9	115.8	118.3	126.0
	$\Delta\delta(Ca_2\text{-apo})$[d]	+14.0	+8.2	+8.2	+5.9
Average	$\Delta\delta$ exp.	+14.5	+6.5	+6.1	+4.3
B: binding of Mg^{2+}					
N-CaM[i]		Ile27	Thr28	Ile63	Asp64
	$\delta(Mg_2)$[b]	121.461	111.356	121.768	n.d.
	δ(apo)[c]	110.636	110.762	118.748	124.835
	$\Delta\delta(Mg_2\text{-apo})$[d]	+10.825	+0.594	+3.020	
C-CaM[j]		Ile100	Ser101	Val136	Asn137
	$\boldsymbol{\delta(Mg_2)}$[b]	l.b.[e]	118.4	l.b.[e]	125.7
	δ(apo)[c]	113.9	118.0	120.0	125.7
	$\Delta\delta(Mg_2\text{-apo})$[d]		+0.4		+0.0
C: mutants of Glu in position 12′ of EF2					
E140Q C-CaM[k]		Ile100	Ser101	Val136	Asn137
	$\delta(Ca_1)$[b]	121.7	120.4	120.0	123.3
	δ(apo)[c]	113.2	117.4	119.3	125.4
	$\Delta\delta(Ca_1\text{-apo})$[d]	+8.5	+3.0	+0.7	−2.1
D: mutants of Glu in position 12 of EF1					
E104Q C-CaM[l]		Ile100	Ser101	Val136	Asn137
	$\delta(Ca_1)$[b]	121.3	120.0	124.3	126.6
	δ(apo)[c]	113.5	117.3	119.6	124.9
	$\Delta\delta(Ca_1\text{-apo})$[d]	+7.8	+2.7	+4.7	+1.7
E41A N-sTnC[m]		Ile37	Ser38	Ile73	Asp74
	$\delta(Ca_1)$[b]	118.5	118.5	128.4	129.9
	δ(apo)[c]	112.4	115.7	118.9	126.6
	$\Delta\delta(Ca_1\text{-apo})$[d]	+6.1	+2.8	+9.5	+3.3
N-cTnC[n]		Ile36	Ser37	Ile72	Asp73
	$\delta(Ca_1)$[b]	119.2	123.2	127.2	128.0
	δ(apo)[c]	113.7	116.0	115.4	124.2
	$\Delta\delta(Ca_1\text{-apo})$[d]	+5.5	+7.2	+11.8	+3.8

[a] Residues in position 8, 9, 8′, 9′: type of residue and numbering correspond to each particular protein. [b] $\delta(Ca_2)$: ^{15}N chemical shift for the NH in $(Ca^{2+})_2$-loaded (holo) form. $\delta(Mg_2)$: ^{15}N chemical shift for the NH in $(Mg^{2+})_2$-loaded form. $\delta(Ca_1)$: ^{15}N chemical shift for the NH in $(Ca^{2+})_1$-loaded form. [c] δ(apo): ^{15}N chemical shift for the NH in Ca^{2+}-free (apo) form. [d] $\Delta\delta(Ca_2\text{-apo})$: ^{15}N chemical shift difference of $(Ca^{2+})_2$-loaded (holo) minus Ca^{2+}-free (apo) forms. $\Delta\delta(Mg_2\text{-apo})$: ^{15}N chemical shift difference of $(Mg^{2+})_2$-loaded minus Ca^{2+}-free (apo) forms. $\Delta\delta(Ca_1\text{-apo})$: ^{15}N chemical shift difference of $(Ca^{2+})_1$-loaded minus Ca^{2+}-free (apo) forms. [e] l.b.: line broadening of the NMR resonances probably originating from conformational exchange. This has prevented the detection of the resonance. [f] Data for holo-CaM taken from ref *79*. [g] Data for apo-CaM from M. Ikura, personal communication (*9*). [h] Data for apo- and holo-TnC taken from ref *80*. [i] A. Malmendal, personal communication (*65*). [j] Data taken from the $^1H/^{15}N$ HSQC spectra shown by Ohki and co-workers (*64*). [k] E140Q C-CaM: E140Q mutant of C-terminal domain of CaM (*57*). [l] E104Q C-CaM: E104Q mutant of C-terminal domain of CaM (*58*). [m] E41A N-sTnC: E41A mutant of the N-terminal domain of skeletal TnC (*59*). [n] N-cTnC: N-terminal domain of cardiac TnC. Data taken from the $^1H/^{15}N$ HSQC spectra shown by Li and co-workers for the N-domain of this protein in the apo and half-saturated states (*61*).

supported experimentally since NOEs between protons on the interacting β-strands are appreciably stronger in the holo state than in the apo state of CaM, where they are either weak or absent (*9*, *36*−*37*). The β-sheet interactions in the C-terminal EF-hand domain of cTnC have also been shown by NH proton chemical shift analysis to be disrupted or weakened in the absence of Ca^{2+} (*38*). Proton exchange rates for the β-sheet amide NH groups in calbindin D_{9k} are observed to decrease upon Ca^{2+} binding, also indicating strengthening of their hydrogen bonds (*39*).

Isoleucine(8) Side Chain Rotation Effect. (i) Calculation of ^{15}N Nuclear Shieldings. The side chain χ_1 torsion angle of isoleucine or valine residues is known to have an effect on ^{15}N chemical shifts. This effect has been analyzed theoretically by De Dios and collaborators (*40*). We have calculated the ^{15}N shieldings in the apo form for both the *gauche(−)* and the trans conformations for isoleucine(8) (Table 1B). The conformational change from *gauche(−)* to *trans* has a deshielding effect on both nitrogens in 8 and 9; the effect is larger for the nitrogen of the isoleucine in position 8 (+7.0 and +4.2 ppm, respectively). The results predict that a 120° variation of the isoleucine χ_1 torsion angle will affect only the nitrogen atoms in residues 8 and 9 with negligible effects on those in residues 8′ and 9′. Our calculated values for the ^{15}N deshielding caused by rotation of the side chain χ_1 torsion angle of isoleucine or valine residues are in good agreement with those shown by De Dios and collaborators (*40*). The side chain χ_1 conformational effect on ^{15}N chemical shifts can also be reproduced by SHIFTX (*41*).

The differences observed in the shielding tensors upon side chain rotation are due to changes in the values of all of its components. However, the changes are not uniform for σ11, σ22, and σ33.

(ii) Comparison with the ^{15}N Experimental Values. The experimental values can be estimated by the differences of the observed shielding values in positions 8 and 9 from the corresponding values in 8′ and 9′ (Table 2A). By doing this, we are assuming that (a) for symmetry reasons, N(8) and N(9) experience a similar polarization deshielding as N(8′) and N(9′) and (b) N(8′) and N(9′) (site EF2) are only affected by polarization deshielding and are independent of the rotamer conformation of site EF1. The estimated experimental values for the *gauche(−)* to *trans* conformational change are $14.5 - 6.1 = +8.4$ ppm for N(8) and $6.5 - 4.3 = +2.2$ ppm for N(9) which follow the same trend as the calculated values +7.0 and +4.2 ppm (Table 1B).

(iii) Origin of the ^{15}N Deshielding Effects. A γ-carbon substituent in a gauche conformation to the nitrogen is known to shield the latter by ca. 5 ppm (*42*). The origin of this γ-effect has been suggested to involve steric compression in the γ-position due to the *gauche* interactions. Grant and Cheeney have proposed that in the case of carbon nuclei, these steric effects are explicable in terms of steric polarization of the valence electrons (*43*). In the *gauche(−)* conformation of our model, N(8) has two γ-carbon substituents in *gauche* conformations to the nitrogen atom, whereas in the *trans* conformation, there is only one. Therefore, the conformational change from *gauche(−)* to *trans* yields a deshielding effect for N(8) in agreement with that observed for the experimental and calculated values.

Table 3: Calculated Bond Lengths for the β-Sheet Amide and Carbonyl Groups in the Holo and Apo Models (A) and Calculated Partial Charges for the Atoms of the β-Sheet Amide Groups in the Holo and Apo Forms (B)

A: Bond Lengths

bond	holo	apo	ΔÅ[a]	bond	holo	apo	ΔÅ[a]
O(7)═C(7)	1.250	1.239	0.011	O(7′)═C(7′)	1.250	1.238	0.012
C(7)−N(8)	1.339	1.356	−0.017	C(7′)−N(8′)	1.339	1.356	−0.017
N(8)−H(8)	1.026	1.023	0.003	N(8′)−H(8′)	1.026	1.023	0.003
H(8)···O(8′)	1.805	1.859	−0.054	H(8′)···O(8)	1.796	1.859	−0.063
O(8′)═C(8′)	1.241	1.240	0.001	O(8)═C(8)	1.241	1.240	0.001
C(8′)−N(9′)	1.340	1.347	−0.007	C(8)−N(9)	1.338	1.347	−0.009
N(9′)−H(9′)	1.028	1.021	0.007	N(9)−H(9)	1.028	1.021	0.007

B: Partial Charges

atom	holo	apo	Δ(holo − apo)	atom	holo	apo	Δ(holo − apo)
O(7)	−0.813	−0.641	−0.172	O(7′)	−0.814	−0.643	−0.171
C(7)	0.702	0.652	+0.050	C(7′)	0.702	0.652	+0.050
N(8)	−0.612	−0.659	+0.047	N(8′)	−0.615	−0.659	+0.044
H(8)	0.470	0.460	+0.010	H(8′)	0.471	0.460	+0.011
O(8)	−0.700	−0.673	−0.027	O(8′)	−0.697	−0.669	−0.028
C(8)	0.663	0.667	−0.004	C(8′)	0.665	0.669	−0.004
N(9)	−0.620	−0.623	+0.003	N(9′)	−0.620	−0.625	+0.005
H(9)	0.464	0.437	+0.027	H(9′)	0.462	0.434	+0.028

[a] Difference between holo and apo bond lengths.

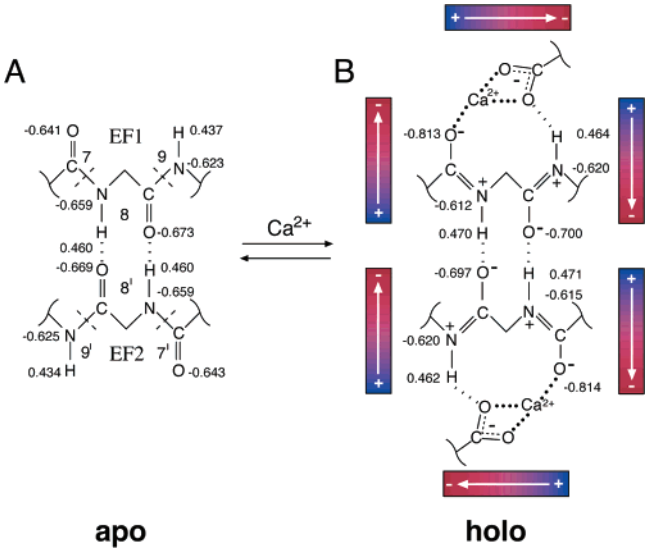

FIGURE 4: Local charge variation upon Ca^{2+} binding. (A) Partial charges calculated for the apo cycle. The glutamates in positions 12 and 12′ are considered at infinite distance and neglected in the calculations. (B) Calculated partial charges of the holo model. Upon Ca^{2+} binding, six dipoles are mutually stabilized in a sequential head-to-tail arrangement forming a circular network of donor-acceptor interactions.

Delocalization Cooperativity. Upon binding Ca^{2+} to both sites, the ^{15}N chemical shifts indicate polarization of the four β-sheet amide groups. These four amide dipoles together with the Ca^{2+}-carboxylate(12) and Ca^{2+}-carboxylate(12′) dipoles form a network of interactions connecting the Ca^{2+} ions across the β-sheet. These six interacting dipoles are sequentially arranged in a head-to-tail fashion to form a circular network as shown in Figure 4B. A similar arrangement of dipoles was proposed by Jeffrey and Saenger in their studies of circular hydrogen bond networks in carbohydrates (*44*−*47*) and also has been found for other hydrogen bond systems (*48*−*50*).

Our preliminary semiempirical calculations (using Cd^{2+} instead of Ca^{2+} as ions) showed that closing this cycle of interactions yields a cooperative stabilization (*30*). In the present work, we have calculated this stabilization energy using ab initio methods on our model incorporating Ca^{2+} ions. After the geometry of the holo system was optimized, the circular network was then split into four groups (two containing the residues at positions 7−9 and 7′−9′ and two containing the residues at positions 12 and 12′, each bound to a Ca^{2+}) (Figure 5). The energies of each of these units and that of the whole circular network were calculated separately. The total donor-acceptor interaction energy of the system is −5.0 kcal/mol smaller than the sum of the isolated interactions.

Thus, the ab initio calculations clearly indicate a cooperative stabilization effect due to the establishment of the circular network connecting the two Ca^{2+} ions across the β-sheet. Although the energies reported here are probably overestimated because they are calculated for fully optimized structures (structures in vacuo), these results are in good agreement with experimental evidence (*12* and references therein). For instance, the Ca^{2+} binding cooperativities measured for both N- and C-terminal domains of CaM are ≥2.4kcal/mol (10 kJ/mol) at 0.15 M KCl (*51*), with a Hill coefficient of 1.33 at low Ca^{2+} concentrations (*52*).

DISCUSSION

Heuristic Power of the Model: Polarization State of the β-Sheet Amide Groups. The chemical shifts of nuclei such as ^{15}N are known to be influenced mostly by local contributions (*40*, *53*, *54*). The minimalist molecular model chosen in this study comprises the main interactions involved in the binding of Ca^{2+} responsible for the observed ^{15}N experimental trends. This model enables the prediction of the polarization states of the four β-sheet amide groups, which indicate the metal occupancy of the Ca^{2+} binding sites in an EF-hand domain as well as the presence or absence of delocalization cooperativity across the β-sheet.

The ab initio calculations show that the two main contributions to the ^{15}N deshielding discussed here, from the polarization and from the isolecine(8) side chain rotation, are additive to a first-order approximation, i.e., $\Delta\delta_{total}(Ni)$

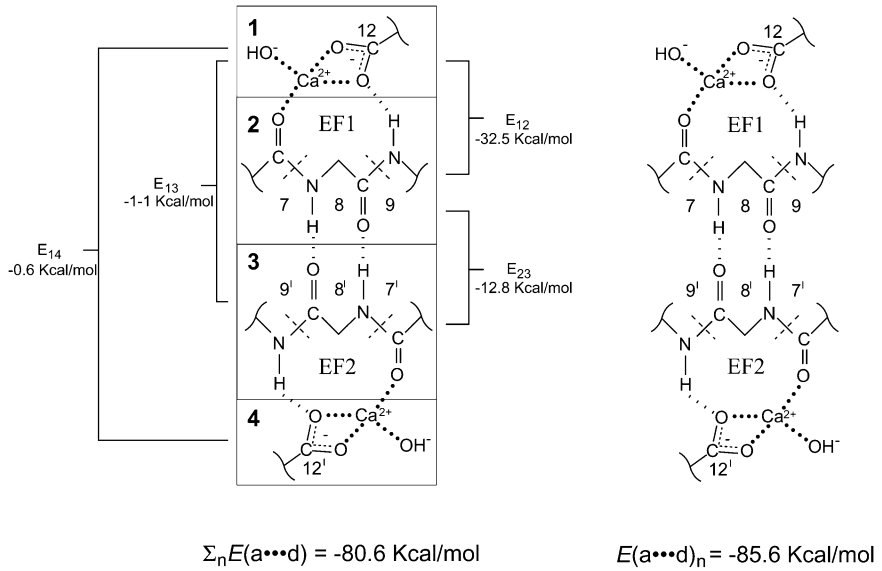

FIGURE 5: Total energy calculated for the individual interactions (left) and for the whole cycle (right). The cycle was split into four components (here indicated as 1, 2, 3, and 4), and the energies of the individual interactions were calculated for all pairs of components. The difference between the total energy of the cycle and the sum of the individual interaction energy represents the cooperativity.

$= \Delta\delta_{\text{polariz}}(\text{N}i) + \Delta\delta_{\text{rotation}}(\text{N}i)$. Table 1C shows that the total effect is the sum of both effects calculated separately, e.g., for N(8) 15.1 + 7.0 ppm = 22.1 ppm. Subtracting $\Delta\delta_{\text{rotation}}(\text{N}i)$ from $\Delta\delta_{\text{total}}(\text{N}i)$, we can determine an experimental value for $\Delta\delta_{\text{polariz}}(\text{N}i)$, the polarization state for each β-sheet amide group, for different EF-hand domains.

To succinctly describe the polarization states of the β-sheet amide groups, we have defined a polarization index P(i) for each of the nitrogens in positions $i = 8, 9, 8', \text{and } 9'$, so that P($i$) = 0 when $\Delta\delta_{\text{polariz}}(\text{N}i) \approx 0$ ppm, and P(i) = 1 when $\Delta\delta_{\text{polariz}}(\text{N}i) \geq 3$ ppm. $\Delta\delta_{\text{polariz}}(\text{N}i)$, the polarization ^{15}N deshielding effect for nitrogen Ni, can be directly correlated with the experimental value, once corrected for the $\Delta\delta_{\text{rotation}}$(N$i$), the side chain χ_1 rotation effect. According to this definition, the polarization state of the β-sheet amide groups can be represented by four numbers [P(8), P(9), P(8′), P(9′)]. For example, for an apo EF-hand domain, the polarization state of the β-sheet is [0, 0, 0, 0], whereas for a holo EF-hand domain it is [1, 1, 1, 1].

We have examined ^{15}N chemical shift data for EF-hand systems from the literature in order to investigate their β-sheet polarization state and, hence, the presence or absence of cooperative stabilization. Three situations of interest have been considered as follows: (i) binding of Mg^{2+}, (ii) mutation of glutamate in position 12′ (site EF2), and (iii) mutation of glutamate in position 12 (site EF1).

(i) Binding of Mg^{2+} to EF-Hand Domains. Analysis of the ^{15}N chemical shift changes induced by Mg^{2+} binding to CaM indicates that although two Mg^{2+} ions each coordinate the carbonyl groups at positions 7 and 7′ (as evidenced by the ^{15}N chemical shift changes in positions 8 and 8′; see Table 2B), Mg^{2+} does not appear to coordinate to the bidentate carboxylates in the glutamate residues at position 12 and 12′, since no ^{15}N chemical shift variations for positions 9 and 9′ are observed on binding Mg^{2+}. Thus, this β-sheet polarization state is [1, 0, 1, 0].

The smaller Mg^{2+} ion is known to bind preferentially to highly negatively charged ligands with strictly 6-fold coordination in an octahedral symmetry (*55*). Unlike Ca^{2+}, Mg^{2+} cannot easily accommodate a bidentate carboxylate (that of position 12) within its sphere of coordination (*55*). Experimentally, the crystal structure of Mg^{2+}-bound calbindin D_{9k} shows that all of the Ca^{2+} ligands of EF2 coordinate with the Mg^{2+} ion, except for the bidentate glutamate, which is replaced by a water molecule (*56*).

(ii) Mutation of Glutamate in Position 12′ of EF2. The ^{15}N chemical shifts of positions 8, 9, 8′, and 9′ in the E140Q mutant of the C-domain of CaM (glutamate in position 12′) are shown in Table 2C (*57*). If the mutation of this residue had resulted in impairment of Ca^{2+} binding in EF2, we would expect no side chain rotation of the isoleucine in position 8 [induced by Ca^{2+} binding to EF2 (*14*)] and no deshielding of N(8′) and N(9′) nitrogens in EF2. This is what is observed experimentally (Table 3); the holo state of this mutant retains the *gauche(−)* conformation for isoleucine(8). The β-sheet polarization state for this EF2 mutant is [1, 1, 0, 0].

(iii) Mutation of Glutamate in Position 12 of EF1. The effect of mutations of position 12 on Ca^{2+} binding can also be analyzed by considering the cases of the E104Q mutant of the C-domain of CaM (*58*) and of the E41A mutant of the N-domain of skeletal TnC (*59*). The NMR data shown in Table 2D indicate that these do not bind Ca^{2+} in EF1. This behavior can be compared with that of the N-domain of wild-type cardiac TnC that also only binds Ca^{2+} in EF2 (*60*, *61*). For these three cases, the nitrogens in positions 8′ and 9′ are deshielded by the polarization due to Ca^{2+} binding to EF2. Ca^{2+} binding to EF2 also results in the 120° χ_1 side chain rotation of the isoleucine in position 8, as reflected by the experimental chemical shift values. The β-sheet polarization state for these cases is thus [0, 0, 1, 1].

Cooperative Stabilization and the Ca^{2+} Switch. Could the cooperative stabilization obtained from establishing a circular network of donor-acceptor interactions be a prerequisite for triggering the Ca^{2+} conformational switch in EF-hand domains?

In the following section, we link the five different polarization states of the β-sheet amide groups observed,

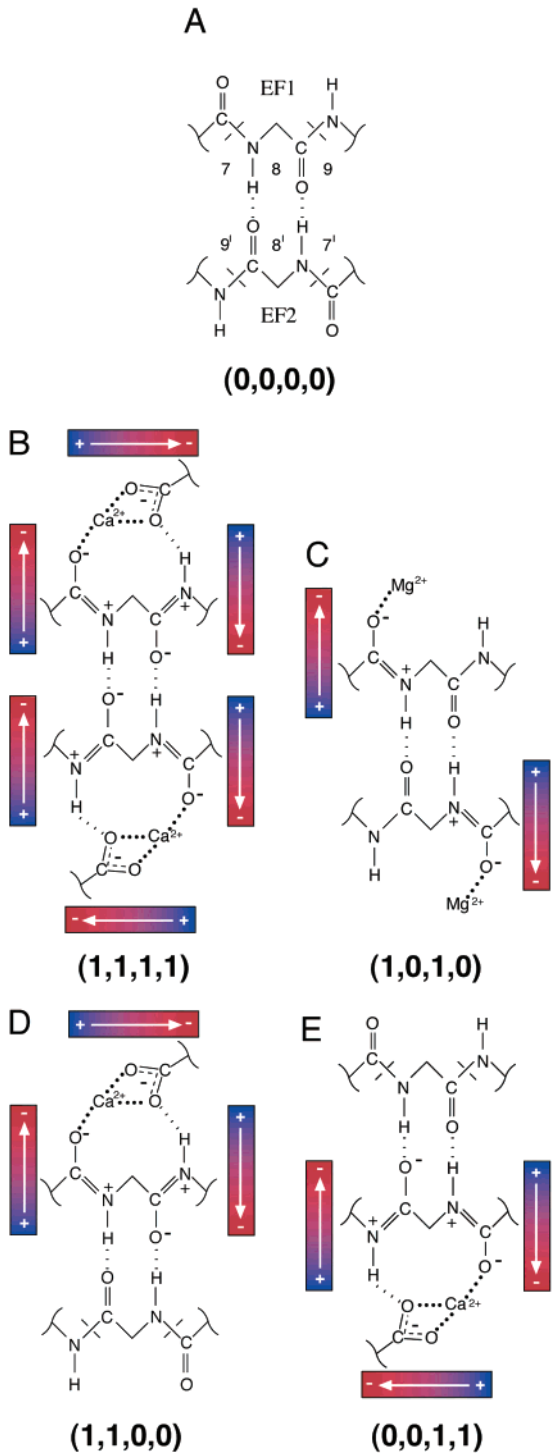

FIGURE 6: Different polarization states of the β-sheet amide groups in the cyclic network indicated as [P(8), P(9), P(8′), P(9′)] where P(i) is defined as a polarization index adopting values 0 or 1 in order to indicate the absence or presence of polarization of the amide group in question as observed from the NMR data. The following five different cases were observed experimentally: (A) [0, 0, 0, 0]; (B) [1, 1, 1, 1]; (C) [1, 0, 1, 0]; (D) [1, 1, 0, 0]; and (E) [0, 0, 1, 1].

namely, [1, 1, 1, 1], [1, 0, 1, 0], [1, 1, 0, 0], [0, 0, 1, 1], and [0, 0, 0, 0] (Figure 6), to their conformational states.

(a) The [0, 0, 0, 0] polarization state corresponds to metal-free EF-hand domains (Figure 6A) known to be in a closed conformation (*7*−*10*, *35*).

(b) The [1, 1, 1, 1] state corresponds to the four β-sheet amide groups being simultaneously polarized as a result of the establishment of the cooperative circular network (Figure 6B). The [1, 1, 1, 1] state is observed when Ca^{2+} binds to both loops of an EF-hand domain and corresponds to an open conformation (*2*, *4*, *62*, *63*).

(c) The [1, 0, 1, 0] state, observed when Mg^{2+} binds to both loops (Figure 6C), corresponds to a closed conformation: Mg^{2+} is known to bind to sensor EF-hand proteins (such as CaM or TnC) without inducing the conformational switch (*64*−*66* and references therein).

(d) Impairing the capability of the glutamate in position 12 or 12′ to coordinate Ca^{2+} in a bidentate manner (for example by mutating the glutamate-12 to glutamine or alanine) also prevents formation of the circular network (Figure 6D). An example is provided by the E140Q mutant in the C-terminal domain of CaM (*57*), which is found in the [1, 1, 0, 0] state. This mutation of position 12′ has been reported to have large effects on the holo conformation of this domain that undergoes rapid exchange between the closed and the open states (*57*).

(e) The [0, 0, 1, 1] state corresponds to the mutants of position 12 and the wild-type cardiac TnC analyzed above (Figure 6E). They have all been reported to be in a closed conformation (*58*−*60*).

Thus, the only case in which a stable "open" conformation has been observed is in the case of [1, 1, 1, 1], when all four β-sheet amide groups are polarized. The emerging hypothesis from this analysis is that the conformational switch and the establishment of the circular network are interconnected and that the cooperative network of interactions is essential for stabilizing the "open" conformation. Impairing the establishment of the cooperative circular network prevents the conformational change from taking place.

The highly conserved glutamate in position 12 plays an essential role in the establishment of the cooperative cycle; hence, its presence is critical for the conformational switch to take place. The invariant glutamate in position 12 forms part of the first turn of the second helix of the EF-hand motif (as shown in Figure 1A). For each Ca^{2+} binding loop, this is the only Ca^{2+} ligand that belongs to one of the EF-hand helices. It can be observed that in apo structures, the carboxylate of the glutamate-12 and -12′ residues are several angstroms farther away from their positions in the respective holo structures as shown in Figure 7. The cooperative stabilization gained by establishing the circular network through the bidentate interaction with the Ca^{2+} ion of both glutamate-12 residues appears to be an essential driving force for exerting the mechanical motion that determines the conformational switch. Metal ions that cannot bind glutamate-12 in a bidentate manner, such as Mg^{2+}, cannot form the cooperative cycle and do not trigger the confomational switch. Mutations that impair the formation of the cooperative cycle (such as position 12 glutamate→glutamine mutations) do not "open" the closed apo conformation upon Ca^{2+} addition.

CONCLUDING REMARKS

In a previous study based on the structural comparison of the closed and open states of an α-spectrin EF-hand domain, we suggested that in the apo state, the glutamate in position 12 of EF1 forms a salt bridge with a conserved lysine in

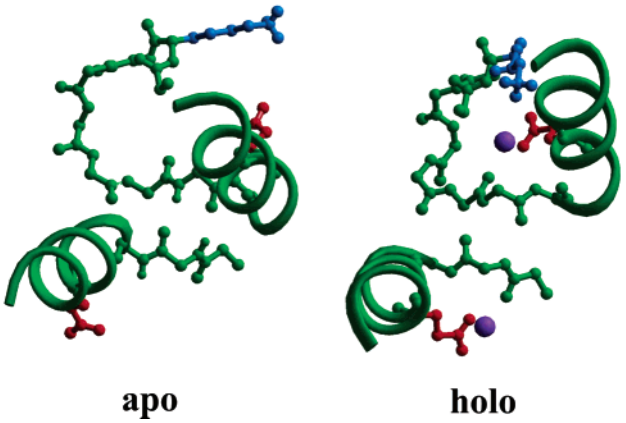

FIGURE 7: Role of the coordination of glutamates in positions 12 and 12′ (shown in red) in the conformational switch: reorientation of the N-terminal EF-hand domain of CaM in (A) the apo [PDB access 1F70 (*35*)] and (B) holo [PDB access 1EXR (*63*)] states. The side chain of the conserved lysine in position 2 of EF1 (shown in light blue) forms a salt bridge with the side chain of glutamate in position 12 in the apo form. Ca^{2+} binding triggers the movements of the glutamate 12 and 12′ side chains that is accompanied by the movement of the second helix (shown in oval representation).

loop position 2 (*67*). This salt bridge would stabilize a closed state of EF1 in the apo form. Upon Ca^{2+} binding, the salt bridge is broken and the EF1 loop stretches adopting a more extended (open) conformation. The cooperative stabilization gained upon establishment of the circular network in the holo form prevails over the stabilization caused by the lysine(2):glutamate(12) salt bridge interaction in the closed apo state. Together with solvation energetics, determined by the subtle interplay of polar and hydrophobic interactions between the pairs of helices (*68*, *69*), the delicate balance between all of these molecular forces ultimately determines the resulting conformation of an EF-hand domain upon the binding of Ca^{2+}.

The ab initio chemical shift calculations presented here provide a theoretical basis to sustain the empirical rules that we had deduced previously (*14*). Thanks to this rationalization, different polarization states for the β-sheet amide groups can be identified and linked to the overall conformation of the EF-hand domain. In this way, the present work establishes a link between circular delocalization stabilization, cooperativity of Ca^{2+} binding, and the "Ca^{2+} switch" conformational change.

MATERIALS AND METHODS

Holo and Apo Models. The holo and apo models used in our calculations are schematically shown in Figures 5 and 4A, respectively. The initial starting structure for the construction of our holo model was the Ca^{2+}-bound structure of the recombinant *Paramecium tetraurelia* CaM at 1.68 Å resolution (PDB accession code 1OSA) (*62*).

The holo model consists of two short β-strands (7−8−9 and 7′−8′−9′) and two Ca^{2+} ions, each with a bidentate carboxylate ligand. In the Ca^{2+}-loaded (holo) form, the carboxylates of the two highly conserved glutamates at the equivalent 12 and 12′ positions (*70*) of the two glutamate residues move close to the β-sheet plane to coordinate Ca^{2+} in a bidentate manner (Figure 2). An OH^- group ligating each Ca^{2+} ion was included for neutrality so that no effects originating from an electrostatic repulsion would arise. Although neglecting three of the seven ligands involved in the bipyramidal penta coordination (i.e., those in positions 1, 3, and 5), this model system was chosen as a computationally manageable and internally neutral fragment that would not require the introduction of counterions.

In the Ca^{2+}-free (apo) form, the carboxylates of the two highly conserved glutamates at the 12 and 12′ positions (*70*) are several angstroms farther away from the rest of the loop (*9*). Hence, these two glutamate residues were not included in the apo model.

Both holo and apo models include the side chains of the conserved isoleucine residues in positions 8 and 8′. Calculations for the apo state were done with conformations *gauche(−)−trans* and *trans−trans*, whereas those for the holo state were done only with the trans−trans conformation.

Computational Methodology. All of the calculations performed in this work were carried out using the Gaussian 98 package (*71*). The geometries of the model systems were fully optimized at the DFT-B3LYP level (*72*, *73*) using the 6-31G** basis set. The BSSE used in the estimated interaction energies were computed using the counterpoise scheme (*74*). It should be noted that all quantities calculated here might be overestimated because of neglecting both the rest of the molecule and the solvent effects. In addition, they were calculated from fully optimized structures in vacuo. Partial charges were computed using a natural population analysis (*75*).

^{15}N Nuclear Shieldings. The ^{15}N chemical shieldings were calculated using the GIAO method (*76*) with a 6-31G** basis set. To calculate absolute values of chemical shifts, isotropic shieldings were also calculated for the reference NH_3 using the same basis set. A value of 18 ppm [^{15}N chemical shift difference between ammonia in the gas and liquid phases (*77*)] was subtracted from the values of the calculated ^{15}N chemical shifts.

Delocalization Cooperativity. The energies of the individual interactions were calculated for all pairs of components in order to estimate $\sum_n E(a\cdots d)$, the sum of the energies of the isolated donor-acceptor interactions, $E(a\cdots d)$. The interaction energy between any two components *i* and *j* was calculated as the energy for *i* and *j* together, *Eij*, minus the energy for the isolated components, *Ei* and *Ej*. The four components taken into account in this work are indicated as 1, 2, 3, and 4 in Figure 3.

ACKNOWLEDGMENT

We are grateful to Claudia Veigel (NIMR, Mill Hill), Pierandrea Temussi (Dipartimento di Chimica, Universita di Napoli Federico II, Naples, Italy), and Paolo Carloni (International School for Advanced Studies, Trieste, Italy) for comments on the manuscript.

REFERENCES

1. Berridge, M. J., Bootman, M. D., and Lipp, P. (1998) Calcium—a life and death signal, *Nature 395*, 645−648.
2. Kretsinger, R. H., and Nockolds, C. E. (1973) Carp muscle calcium-binding protein. II. Structure determination and general description, *J. Biol. Chem. 248*, 3313−3326.
3. Tsalkova, T. N., and Privalov, P. L. (1985) Thermodynamic study of domain organization in troponin C and calmodulin, *J. Mol. Biol. 181*, 533−544.

4. Herzberg, O., and James. M. N. G (1985) Structure of the calcium regulatory muscle protein troponin-C at 2.8 Å resolution, *Nature 313*, 653−659.
5. Schutt, C. (1985) Hands on the calcium switch, *Nature 315*, 15−15.
6. Herzberg, O., Moult, J., and James, M. N. (1986) A model for the Ca^{2+}-induced conformational transition of troponin C. A trigger for muscle contraction, *J. Biol. Chem. 261*, 2638−2644.
7. Kuboniwa, H., Tjandra, N., Grzesiek, S., Ren, H., Klee, C. B., and Bax, A. (1995) Solution structure of calcium-free calmodulin, *Nat. Struct. Biol. 2*, 768−776.
8. Finn, B. E., Evenäs, J., Drakenberg, T., Waltho, J. P., Thulin, E., and Forsén, S. (1995) Calcium-induced structural changes and domain autonomy in calmodulin, *Nat. Struct. Biol. 2*, 777−783.
9. Zhang, M., Tanaka, T., and Ikura, M. (1995) Calcium-induced conformational transition revealed by the solution structure of apo calmodulin, *Nat. Struct. Biol. 2*, 758−767.
10. Gagné, S. M., Tsuda, S., Li, M. X., Smillie, L. B., and Sykes, B. D. (1995) Structures of the troponin C regulatory domains in the apo- and calcium-saturated states, *Nat. Struct. Biol. 2*, 784−789.
11. Hoeflich, K. P., and Ikura, M. (2002) Calmodulin in action: diversity in target recognition and activation mechanisms, *Cell 108*, 739−742.
12. Linse, S., and Chazin, W. J. (1995) Qunatitative measurements of the cooperativity in an EF-hand protein with sequential calcium binding, *Protein Sci. 4*, 1038−1044.
13. Kawasaki, H., and Kretsinger, R. H. (1994) Calcium-binding proteins. 1: EF-hands, *Protein Profile 1*, 343−517.
14. Biekofsky, R. R., Martin, S. R., Browne, J. P., Bayley, P. M., and Feeney, J. (1998) Ca^{2+} coordination to backbone carbonyl oxygen atoms in calmodulin and other EF-hand proteins: ^{15}N chemical shifts as probes for monitoring individual-site Ca^{2+} coordination, *Biochemistry 37*, 7617−7629.
15. Matei, E., Miron, S., Blouquit, Y., Duchambon, P., Durussel, I., Cox, J. A., and Craescu, C. T. (2003) C-terminal half of human centrin 2 behaves like a regulatory EF-hand domain, *Biochemistry 42*, 1439−1450.
16. Theret, I., Baladi, S., Cox, J. A., Gallay, J., Sakamoto, H., and Craescu, C. T. (2001) Solution structure and backbone dynamics of the defunct domain of calcium vector protein, *Biochemistry 40*, 13888−13897.
17. Atreya, H. S., Sahu, S. C., Bhattacharya, A., Chary, K. V. R., and Govil, G. (2001) NMR derived solution structure of an EF-hand calcium-binding protein from *Entamoeba histolytica*, *Biochemistry 40*, 14392−14403.
18. Wijesinha-Bettoni, R., Dobson, C. M., and Redfield, C. (2001) Comparison of the structural and dynamical properties of holo and apo bovine alpha-lactalbumin by NMR spectroscopy, *J. Mol. Biol. 307*, 885−898.
19. Lytle, B. L., Volkman, B. F., Westler, W. M., and Wu, J. H. D. (2000) Secondary structure and calcium-induced folding of the *Clostridium thermocellum* dockerin domain determined by NMR spectroscopy, *Arch. Biochem. Biophys. 379*, 237−244.
20. Enmon, J. L., de Beer, T., and Overduin, M. (2000) Solution structure of Eps15's third EH domain reveals coincident Phe-Trp and Asn-Pro-Phe binding sites, *Biochemistry 39*, 4309−4319.
21. Dolmer, K., Huang, W., and Gettins, P. G. W. (2000) NMR solution structure of complement-like repeat CR3 from the low-density lipoprotein receptor-related protein—evidence for specific binding to the receptor binding domain of human alpha(2)-macroglobulin, *J. Biol. Chem. 275*, 3264−3269.
22. Whitehead, B., Tessari, M., Carotenuto, A., Henegouwen, P. M. P. V. E., and Vuister, G. W. (1999) The EH1 domain of Eps15 is structurally classified as a member of the S100 subclass of EF-hand-containing proteins, *Biochemistry 38*, 11271−11277.
23. Huang, W., Dolmer, K., and Gettins, P. G. W. (1999) NMR solution structure of complement-like repeat CR8 from the low-density lipoprotein receptor-related protein, *J. Biol. Chem. 274*, 14130−14136.
24. Dolmer, K., Huang, W., and Gettins, P. G. W. (1998) Characterization of the calcium site in two complement-like domains from the low-density lipoprotein receptor-related protein (LRP) and comparison with a repeat from the low-density lipoprotein receptor, *Biochemistry 37*, 17016−17023.
25. Lee, H. W., Yang, W., Ye, Y. M., Liu, Z. R., Glushka, J., and Yang, J. J. (2002) Isolated EF-loop III of calmodulin in a scaffold protein remains unpaired in solution using pulsed-field-gradient NMR spectroscopy, *Biochim. Biophys. Acta 1598*, 80−87.
26. Li, M. X., Saude, E. J., Wang, X., Pearlstone, J. R., Smillie, L. B., and Sykes, B. D. (2002) Kinetic studies of calcium and cardiac troponin I peptide binding to human cardiac troponin C using NMR spectroscopy, *Eur. Biophys. J. 31*, 245−256.
27. Jaren, O. R., Kranz J. K., Sorensen, B. R., Wand, A. J., and Shea, M. A. (2002) Calcium-induced conformational switching of Paramecium calmodulin provides evidence for domain coupling, *Biochemistry 41*, 14158−14166.
28. Mercier, P., Li, M. X., and Sykes, B. D. (2000) Role of the structural domain of troponin C in muscle regulation: NMR studies of Ca^{2+} binding and subsequent interactions with regions 1−40 and 96−115 of troponin I, *Biochemistry 39*, 2902−2911.
29. Fefeu, S., Biekofsky, R. R., McCormick, J. E., Martin, S. R., Bayley, P. M., and Feeney, J. (2000) Calcium-induced refolding of the calmodulin V136G mutant studied by NMR spectroscopy: Evidence for interaction between the two globular domains, *Biochemistry 39*, 15920−15931.
30. Biekofsky, R. R., and Feeney, J. (1998) Cooperative cyclic interactions involved in metal binding to pairs of sites in EF-hand proteins, *FEBS Lett. 439*, 101−106.
31. Szilagyi, L. (1995) Chemical shifts in proteins come of age, *Prog. Nucl. Magn. Reson. Spectrosc. 27*, 325−443.
32. Williamson, M. P., and Asakura, T. (1997) Protein chemical shifts, *Methods Mol. Biol. 60*, 53−69.
33. Case, D. A. (2000) Interpretation of chemical shifts and coupling constants in macromolecules, *Curr. Opin. Struct. Biol. 10*, 197−203.
34. Wishart, D. S., and Case, D. A. (2001) Use of chemical shifts in macromolecular structure determination, *Methods Enzymol. 338*, 3−34.
35. Chou, J., Li, S., and Bax, A. (2001) Study of conformational rearrangement and refinement of structural homology models by the use of heteronuclear dipolar couplings, *J. Biomol. NMR 18*, 217−227.
36. Ikura, M., Minowa, O., and Hikichi, K. (1985) Hydrogen bonding in the carboxyl-terminal half-fragment 78−148 of calmodulin as studied by two-dimensional nuclear magnetic resonance, *Biochemistry 24*, 4264−4269.
37. Urbauer, J. L., Short, J. H., Dow, L. K., and Wand, A. J. (1995) Structural analysis of a novel interaction by calmodulin: high-affinity binding of a peptide in the absence of calcium, *Biochemistry 34*, 8099−8109.
38. Krudy, G. A., Brito, R. M. M., Putkey J. A., and Rosevear, P. R. (1992) Conformational changes in the metal-binding sites of cardiac troponin C induced by calcium binding, *Biochemistry 31*, 1595−1602.
39. Linse, S., Teleman, O., and Drakenberg, T. (1990) Ca^{2+} binding to calbindin D9k strongly affects backbone dynamics: measurements of exchange rates of individual amide protons using ^{1}H NMR, *Biochemistry 29*, 5925−5934.
40. De Dios, A. C., Pearson, J. G., and Oldfield, E. (1993) Secondary and tertiary structural effects on protein NMR chemical shifts: an ab initio approach, *Science 260*, 1491−1496.
41. Neal, S., Nip, A. M., Zhang, H., and Wishart, D. S. (2003) Rapid and accurate calculation of protein ^{1}H, ^{13}C and ^{15}N chemical shifts, *J. Biomol. NMR 26*, 215−40.
42. Le, H., and Oldfield, E. (1994) Correlation between ^{15}N NMR chemical shifts in proteins and secondary structure, *J. Biomol. NMR 4*, 341−348.
43. Grant, D. M., and Cheney, B. V. (1967) Carbon-13 magnetic resonance. VII. Steric perturbation of the carbon-13 chemical shift, *J. Am. Chem. Soc. 89*, 5315−5318.
44. Lesyng, B., and Saenger, W. (1981) Theoretical investigations on circular and chainlike hydrogen bonded structures found in two crystal froms of α-cyclodextrin hexahydrate. Models for hydration and water clusters, *Biochim. Biophys. Acta 678*, 408−413.
45. Koehler, J. E. H., Lesyng, B., and Saenger, W. (1987) Cooperative effects in extended hydrogen bonded systems involving OH-groups. *Ab initio* studies of the cyclic S_4 water tetramer, *J. Comput. Chem. 8*, 1090−1098.
46. Saenger, W. (1979) Circular hydrogen bonds, *Nature (London) 279*, 343−344.
47. Jeffrey, G. A., and Saenger W. (1991) *Hydrogen Bonding in Biological Structures*, Springer-Verlag, Berlin, Heidelberg.
48. Maes, G., and Smets, J. (1993) Hydrogen bond cooperativity—a quantitative study using matrix-isolation FT-IR spectroscopy. *J. Phys. Chem. 97*, 1818−1825.

49. Cruzan, J. D., Brally, L. B., Liu, K., Brown, M. G., Loeser, J. G., and Saykally, R. J. (1996) Quantifying hydrogen-bond cooperativity in water—VRT spectroscopy of the water tetramer. *Science 271*, 59−62.
50. Estrin, D. A., Paglieri, L., Corongiu, G., and Clementi, E. (1996) On small clusters of water molecules using density functional theory. *J. Phys. Chem. 100*, 8701−8711.
51. Linse, S., Helmersson, A., and Forsén, S. (1991) Calcium binding to calmodulin and its globular domains, *J. Biol. Chem. 266*, 8050−8054.
52. Crouch, T. H., and Klee, C. B. (1980) Positive cooperative binding of calcium to bovine brain calmodulin, *Biochemistry 19*, 3692−3698.
53. Levy, G. C., and Lichter, R. L. (1979) *Nitrogen-15 NMR Spectroscopy*, Wiley-Interscience, New York.
54. Witanowski, M., Stefaniak, L., and Webb, G. A. (1993) Nitrogen NMR spectroscopy, *Annu. Rep. NMR Spectrosc. 25*, 2−469.
55. Fraústo da Silva, J. J. R., and Williams, R. J. P. (1991) *The Biological Chemistry of the Elements*, Clarendon Press, Oxford.
56. Andersson, M., Malmendal, A., Linse, S., Ivarsson, I., Forsén, S., and Svensson, L. A. (1997) Structural basis for the negative allostery between Ca^{2+}- and Mg^{2+}-binding in the intracellular Ca^{2+}-receptor calbindin D9k, *Protein Sci. 6*, 1139−1147.
57. Evenäs, J., Thulin, E., Malmendal, A., Forsén, S., and Carlström, G. (1997) NMR studies of the E140Q mutant of the carboxy-terminal domain of calmodulin reveal global conformational exchange in the Ca^{2+}-saturated state, *Biochemistry 36*, 3448−3457.
58. Evenäs, J., Malmendal, A., Thulin, E., Carlström, G., and Forsén, S. (1998) Ca^{2+} binding and conformational changes in a calmodulin domain, *Biochemistry 37*, 13744−13754.
59. Gagné, S. M., Li, M. X., and Sykes, B. D. (1997) Mechanism of direct coupling between binding and induced structural change in regulatory calcium binding proteins, *Biochemistry 36*, 4386−4392.
60. Spyracopoulos, L., Li, M. X., Sia, S. K., Gagné, S. M., Chandra, M., Solaro, R. J., and Sykes, B. D. (1997) Calcium-induced structural transition in the regulatory domain of human cardiac troponin C, *Biochemistry 36*, 12138−12146.
61. Li, M. X., Gagné, S. M., Spyracopoulos, L., Kloks, C. P. A. M., Audette, G., Chandra, M., Solaro, R. J., Smillie, L. B., and Sykes, B. D. (1997) NMR studies of Ca^{2+} binding to the regulatory domains of cardiac and E41A skeletal muscle troponin C reveal the importance of site I to energetics of the induced structural changes, *Biochemistry 36*, 12519−12525.
62. Ban, C., Ramakrishnan, B., Ling, K. Y., Kung, C., and Sundaralingam, M. (1994) Structure of the recombinant *Paramecium tetraurelia* calmodulin at 1.68 Å resolution, *Acta Crystallog. Sect. D: Biol. Crystallogr. 50*, 50−63.
63. Wilson, M. A., and Brunger, A. T. (2000) The 1.0 Å crystal structure of Ca^{2+}-bound calmodulin: an analysis of disorder and implications for functionally relevant plasticity, *J. Mol. Biol. 301*, 1237−1256.
64. Ohki, S., Ikura, M., and Zhang, M. (1997) Identification of Mg^{2+}-binding sites and the role of Mg^{2+} on target recognition by calmodulin, *Biochemistry 36*, 4309−4316.
65. Malmendal, A., Evenäs, J., Thulin, E., Gippert, G. P., Drakenberg, T., and Forsén, S. (1998) When size is important. Accommodation of magnesium in a calcium binding regulatory domain, *J. Biol. Chem. 273*, 28994−29001.
66. Martin, S. R., Masino, L., and Bayley, P. M. (2000) Enhancement by Mg^{2+} of domain specificity in Ca^{2+}-dependent interactions of calmodulin with target sequences, *Protein Sci. 9*, 2477−2488.
67. Travé, G., Lacombe, P. J., Pfuhl, M., Saraste, M., and Pastore, A. (1995) Molecular mechanism of the calcium-induced conformational change in the spectrin EF-hands, *EMBO J. 14*, 4922−4931.
68. Ababou, A., and Desjarlais, J. R. (2001) Solvation energetics and conformational change in EF-hand proteins, *Protein Sci. 10*, 301−312.
69. Ababou, A., Shenvi, R. A., and Desjarlais, J. R. (2001) Long-range effects on calcium binding and conformational change in the N-domain of calmodulin, *Biochemistry 40*, 12719−12726.
70. Moncrief, N. D., Kretsinger, R. H., and Goodman, M. (1990) Evolution of EF-hand calcium-modulated proteins. I. Relationships based on amino acid sequences, *J. Mol. Evol. 30*, 522−562.
71. Frisch, M. J., Trucks, G. W., Schlegel, H. B., Scuseria, G. E., Robb, M. A., Cheeseman, J. R., Zakrzewski, V. G., Montgomery, J. A., Jr., Stratmann, R. E., Burant, J. C., Dapprich, S., Millam, J. M., Daniels, A. D., Kudin, K. N., Strain, M. C., Farkas, O., Tomasi, J., Barone, V., Cossi, M., Cammi, R., Mennucci, B., Pomelli, C., Adamo, C., Clifford, S., Ochterski, J., Petersson, G. A., Ayala, P. Y., Cui, Q., Morokuma, K., Salvador, P., Dannenberg, J. J., Malick, D. K., Rabuck, A. D., Raghavachari, K., Foresman, J. B., Cioslowski, J., Ortiz, J. V., Baboul, A. G., Stefanov, B. B., Liu, G., Liashenko, A., Piskorz, P., Komaromi, I., Gomperts, R., Martin, R. L., Fox, D. J., Keith, T., Al-Laham, M. A., Peng, C. Y., Nanayakkara, A., Gonzalez, C., Challacombe, M., Gill, P. M. W., Johnson, B., Chen, W., Wong, M. W., Andres, J. L., Gonzalez, C., Head-Gordon, M., Replogle, E. S., and Pople, J. A. (1998) *GAUSSIAN 98*, Rev. A7, Gaussian Inc., Pittsburgh, PA.
72. Becke, A. D. (1993) Density-functional thermochemistry 3. The role of exact exchange, *J. Chem. Phys. 98*, 5648−5652.
73. Lee, C., Yang, W., and Parr, R. (1988) Development of the Colle-Salvetti correlation energy formula into a functional of the electron density, *Phys. Rev. B 37*, 785−789.
74. Boys, S. F., and Bernardi, F. (1970) The calculation of small molecular interactions by the differences of separate total energies. Some procedures with reduced errors, *Mol. Phys. 19*, 553−566.
75. Glendening, E. D., Reed, A. E., Carpenter, J. E., and Weinhold, F. *NBO*, version 3.1, Theoretical Chemistry Institute and Department of Chemistry, University of Wisconsin, Madison, WI.
76. Wolinski, K., Hinton, J. F., and Pulay, P. (1990) Efficient implementation of the gauge-independent atomic orbital method for NMR chemical shift calculations, *J. Am. Chem. Soc. 112*, 8251−8260.
77. Martin, G. L., Martin, M. L., and Gouesnard, J.-P. (1981) ^{15}N-NMR spectroscopy. in *NMR Basic Principles and Progress 50* (Diehl, P., Fluck, E., and Kostfeld, R., Eds.) Springer, Berlin.
78. Strynadka, N. C. J., and James, M. N. G. (1989) Crystal structures of the helix-loop-helix calcium-binding proteins, *Annu. Rev. Biochem. 58*, 951−998.
79. Ikura, M., Kay, L. E., and Bax, A. (1990) A novel approach for sequential assignment of ^{1}H, ^{13}C, and ^{15}N spectra of proteins: heteronuclear triple-resonance three-dimensional NMR spectroscopy. Application to calmodulin, *Biochemistry 29*, 4659−4667.
80. Li, M. S., Gagné, S. M., Tsuda, S., Kay, C. M., Smillie, L. B., and Sykes, B. D. (1995) Calcium binding to the regulatory N-domain of skeletal muscle troponin C occurs in a stepwise manner, *Biochemistry 34*, 8330−8340.

BI0497852